Improving reflectivity using linearized waveform inversion with velocity updating

Alejandro Cabrales-Vargas

ABSTRACT

In this report I show how linearized waveform inversion with velocity updating can correct the estimated reflectivity amplitude in the presence of residual inaccuracies in the velocity field, in contrast to conventional linearized waveform inversion.

INTRODUCTION

Linearized waveform inversion with velocity updating (LWIVU) (Cabrales-Vargas et al., 2016, 2017; Cabrales-Vargas, 2017) was proposed as an alternative to conventional linearized waveform inversion (LWI) when small velocity inaccuraries in the velocity model affect the amplitudes in the estimated reflectivity image. In this report I refer to LWI as the *least-squares migration* process performed in *model space* (Valenciano et al., 2006; Tang, 2011) to differentiate it from the well known method performed in *data space* (Nemeth and Schuster, 1999; Schuster, 2017).

In the following section I provide a succint review of LWIVU with the up-to-date features. Next, I describe the preliminar steps for the synthetic examples shown afterwards. Finally, I present the conclusions and discuss future steps.

BRIEF REVIEW OF LWIVU

Definition

We first assume that the subsurface properties model, $\mathbf{m}$, can be express as the summation of a background component, $\mathbf{b}$, and a reflectivity component, $\mathbf{r}$,

$$\mathbf{m} = \mathbf{b} + \mathbf{r},$$

which we can separate into low-wavenumber components (background), $\mathbf{b}_0$, $\mathbf{r}_0$, and high-wavenumber components (perturbation), $\mathbf{\Delta b}$, $\mathbf{\Delta r}$:

$$\mathbf{b} = \mathbf{b}_0 + \mathbf{\Delta b},$$
$$\mathbf{r} = \mathbf{r}_0 + \mathbf{\Delta r}.$$

Assuming smooth transitions in the subsurface model we can drop the background reflectivity component, $\mathbf{r}_0$, (Barnier and Almomin, 2014), obtaining

$$\mathbf{m} = \mathbf{b}_0 + \mathbf{\Delta b} + \mathbf{\Delta r}. \tag{1}$$

I indistinctly refer to $\mathbf{\Delta r}$ both as "the reflectivity" or "the perturbation in the reflectivity" throughout this report. Henceforth, the subsurface model represents slowness squared, $\mathbf{m} = \mathbf{s}^2$.

Now consider the full-waveform inversion (FWI) misfit function, $\Phi(\mathbf{m})$, given by:

$$\Phi(\mathbf{m}) = \frac{1}{2}\|\mathcal{L}(\mathbf{m}) - \mathbf{d}_r\|_2^2, \tag{2}$$

where $\mathcal{L}(\mathbf{m})$ is the non-linear acoustic wave propagation operator, and $\mathbf{d}_r$ represents the recorded data.

We can *locally* linearize the FWI objective function by locally fitting a quadratic function, and update the model towards the corresponding minimum given as $\mathbf{m} = \mathbf{m}_0 + \delta\mathbf{m}$, where $\mathbf{m}_0$ is the current model, and $\delta\mathbf{m}$ is an updating increment that satisfies $\|\delta\mathbf{m}\| << \|\mathbf{m}_0\|$. Expanding the gradient of the FWI objective function in Taylor's series around $\mathbf{m}_0$ we obtain

$$\nabla\Phi(\mathbf{m}) = \mathbf{0} \approx \nabla\Phi(\mathbf{m}_0) + \mathbf{H}(\mathbf{m}_0)\delta\mathbf{m},$$

where $\mathbf{H}$ represents the FWI *full* Hessian. The gradient, $\nabla\Phi(\mathbf{m})$, vanishes because it is evaluated at a minimum. The last expression represents the Newton's equation, typically cast as

$$\mathbf{H}(\mathbf{m}_0)\delta\mathbf{m} = -\nabla\Phi(\mathbf{m}_0). \tag{3}$$

Each FWI iteration demands solving equation 3 to find $\delta\mathbf{m}$, representing a linear minimization problem.

According to Biondi et al. (2015), the FWI full Hessian can be expressed as the summation of the FWI Gauss-Newton Hessian, $\mathbf{H}_{GN}$ (henceforth referred to as "the Hessian"), and the wave-equation migration velocity analysis (WEMVA) operator, $\mathbf{W}$,

$$\mathbf{H} = \mathbf{H}_{GN} + \mathbf{W}. \tag{4}$$

On the other hand, let us assume that in the Newton's equation the current model is given by the most background model, $\mathbf{m}_0 = \mathbf{b}_0$, while the update term encompasses the perturbations in the background and in the reflectivity, $\delta\mathbf{m} = \mathbf{\Delta b} + \mathbf{\Delta r}$. Substituting these expressions and equation 4 into equation 3 we obtain

$$\big[\mathbf{H}_{GN}(\mathbf{b}_0) + \mathbf{W}(\mathbf{b}_0)\big]\big[\mathbf{\Delta b} + \mathbf{\Delta r}\big] = -\nabla\Phi(\mathbf{b}_0). \tag{5}$$

The right-hand side term of equation 5 can be obtained by evaluating $\nabla\Phi(\mathbf{m})$ at $\mathbf{b}_0$:

$$\nabla\Phi(\mathbf{b}_0) = \left[\frac{d\mathcal{L}(\mathbf{b}_0)}{d\mathbf{m}}\right]'\big[\mathcal{L}(\mathbf{b}_0) - \mathbf{d}_r\big], \tag{6}$$

where $\prime$ represents the adjoint of the operator inside the square parentheses. Note that $\mathbf{\Delta d} = \mathbf{d}_r - \mathcal{L}(\mathbf{b}_0)$ is the perturbation in the data (Barnier and Almomin, 2014), *i.e.*, the recorded data after removing direct waves. The derivative of $\mathcal{L}$ with respect to model parameters evaluated at $\mathbf{b}_0$ constitutes the Born modeling operator, hence the adjoint operator represents *migration*. Thus,

$$\nabla\Phi(\mathbf{b}_0) = -\mathbf{\Delta r}_m,$$

where I represent the migration image as $\mathbf{\Delta r}_m$ to regard it as the first estimation of the perturbation in the reflectivity, $\mathbf{\Delta r}$. Substituting the last expression into equation 5, dropping the dependance on $\mathbf{b}_0$ to simplify notation, expanding and re-acommodating terms, we obtain

$$\big[\mathbf{H}_{GN}\mathbf{\Delta r} + \mathbf{W}\mathbf{\Delta b}\big] + \big[\mathbf{H}_{GN}\mathbf{\Delta b} + \mathbf{W}\mathbf{\Delta r}\big] = \mathbf{\Delta r}_m. \tag{7}$$

The first term in the left-hand side of equation 7 is usually employed in conventional LWI to minimize $\|\mathbf{H}_{GN}\mathbf{\Delta r} - \mathbf{\Delta r}_m\|_2^2$. The second term translates perturbations in the background into perturbations in the image. I preserve this term to correct the reflectivity for the inaccuracies in the slowness squared field, and disregard the following ones which presumably account for nonlinear effects such as multi-scattering. Therefore, the LWIVU method is based on the fitting goal $\mathbf{H}_{GN}\mathbf{\Delta r} - \mathbf{W}\mathbf{\Delta b} - \mathbf{\Delta r}_m \approx \mathbf{0}$, corresponding to the objective function

$$\Phi(\mathbf{\Delta r}, \mathbf{\Delta b}; \mathbf{b}_0) = \frac{1}{2}\big\|\mathbf{H}_{GN}\mathbf{\Delta r} - \mathbf{W}\mathbf{\Delta b} - \mathbf{\Delta r}_m\big\|_2^2 - \frac{\lambda^2}{2}\big\|\mathbf{W}\mathbf{\Delta b} + \mathbf{\Delta r}_m\big\|_2^2, \tag{8}$$

where the second term *maximizes* the stacking or energy power of the migrated image as a function of $\mathbf{\Delta b}$ (note the minus sign), and λ is a parameter that allows one to control the influence of such term. Note that I flipped the sign of the $\mathbf{W}\mathbf{\Delta b}$ term to obtain the correct sign of the anomaly. This strategy does not affect the result.

My goal is to obtain a better estimation of the reflectivity, $\mathbf{\Delta r}$, in comparison to conventional LWI. By incorporating inaccuracies in the slowness squared field as perturbations in the migration image by means of WEMVA, $\mathbf{W}\mathbf{\Delta b}$, the current migration image, $\mathbf{\Delta r}_m$, is improved. Thus, the perturbation in the reflectivity is fitted to such an improved migration image during the inversion process.

Data space and model space

It is important to identify the *data space* and the *model space* in LWIVU. The latter is obviously constituted by the subspaces spanned by the perturbations $\mathbf{\Delta r}$ and $\mathbf{\Delta b}$.

To identify the data space, let us first obtain the gradient, *i.e.*, the derivative of the

LWIVU objective function with respect to the model parameters. From equation 8,

$$\nabla\Phi = \begin{bmatrix} \nabla_{\mathbf{\Delta r}}\Phi \\ \nabla_{\mathbf{\Delta b}}\Phi \end{bmatrix} = \begin{bmatrix} \mathbf{H}'\big[\mathbf{H\Delta r} - \big(\mathbf{\Delta r}_m + \mathbf{W\Delta b}\big)\big] \\ -\mathbf{W}'\big[\mathbf{H\Delta r} - \big(\mathbf{\Delta r}_m + \mathbf{W\Delta b}\big)\big] - \lambda^2\mathbf{W}'\big[\mathbf{\Delta r}_m + \mathbf{W\Delta b}\big] \end{bmatrix}$$

$$= \begin{bmatrix} \mathbf{H}' & \mathbf{0} \\ -\mathbf{W}' & -\lambda^2\mathbf{W}' \end{bmatrix} \begin{bmatrix} \mathbf{H\Delta r} - \big(\mathbf{\Delta r}_m + \mathbf{W\Delta b}\big) \\ \mathbf{\Delta r}_m + \mathbf{W\Delta b} \end{bmatrix}. \tag{9}$$

The rightmost term in equation 9 shows the application of the "adjoint" matrix to the residual vector. Quotes stand because true forward and adjoint operators cannot be explicitly obtained. Such residual vector has both components in the domain of the migration image. In fact, the term $\mathbf{H\Delta r}$ projects reflectivity onto such a domain, and $\mathbf{W\Delta b}$ constitutes a perturbation in the image as previously mentioned.

We can further factorize the residual to obtain

$$\begin{bmatrix} \mathbf{H}' & \mathbf{0} \\ -\mathbf{W}' & -\lambda^2\mathbf{W}' \end{bmatrix} \left\{ \begin{bmatrix} \mathbf{H} & -\mathbf{W} \\ \mathbf{0} & \mathbf{W} \end{bmatrix} \begin{bmatrix} \mathbf{\Delta r} \\ \mathbf{\Delta b} \end{bmatrix} - \begin{bmatrix} \mathbf{\Delta r}_m \\ -\mathbf{\Delta r}_m \end{bmatrix} \right\} = \begin{bmatrix} \mathbf{0} \\ \mathbf{0} \end{bmatrix}. \tag{10}$$

Note that from equation 10, if the initial model, $[\mathbf{\Delta r}_0 \quad \mathbf{\Delta b}_0]^T$, is set to zero, the input data for LWIVU become

$$\mathbf{d} = \begin{bmatrix} \mathbf{\Delta r}_m \\ -\mathbf{\Delta r}_m \end{bmatrix}, \tag{11}$$

which simply consists of the migration image and its negative. Therefore, the data space is composed by two subspaces of the migration image domain.

EXPERIMENT SETUP

I performed a numerical experiment to test how LWIVU potentially corrects amplitudes when small velocity inaccuracies remain. In the following I use velocity in the plots for better understanding, although the subsurface model is formally defined in terms of slowness squared.

I built a two-layer model with two Gaussian velocity anomalies of opposite polarity shown in Figure 1a, which represents the true slowness squared model, $\mathbf{m}$. The anomalies in velocity are shown Figure 1b. The minimum and maximum velocities of the anomalies are -50 and 50 m/s, corresponding to a 2% variation with respect to the upper layer (2000 m/s.) The premise of the method is that the inaccuracies of velocity (or slowness squared) are small enough that solely alter the amplitude of the events, not their position, thus justifying the linearity of LWIVU. I obtained the background slowness squared field, $\mathbf{b}$, by smooting the reflector and keeping the anomalies. The corresponding reflectivity, $\mathbf{\Delta r}$, is obtained by subtracting $\mathbf{b}$ from $\mathbf{m}$ (see equation 1.) The most background model, $\mathbf{b}_0$, can be obtained by removing the Gaussian anomalies, $\mathbf{\Delta b}$, from $\mathbf{b}$. Note that $\mathbf{\Delta b}$ represents the anomalies in slowness squared (Figure 9b), not in velocity.

I synthesized the perturbation in the data, $\mathbf{\Delta d} = \mathbf{S}\big[\mathcal{L}(\mathbf{m}) - \mathcal{L}(\mathbf{m}_s)\big]$, where $\mathbf{m}_s$ represents slowness squared at the surface employed to model direct waves for their removal from $\mathcal{L}(\mathbf{m})$, and operator $\mathbf{S}$ samples the wavefield at the surface. These data constitute the input shot gathers that carry information about the anomalies. I also synthesized a second dataset, $\mathbf{\Delta d}_0 = \mathbf{S}\big[\mathcal{L}(\mathbf{m}_0) - \mathcal{L}(\mathbf{m}_s)\big]$, where $\mathbf{m}_0 = \mathbf{b}_0 + \mathbf{\Delta r}$ incorporates the edge of the reflector, *but not the anomalies*. Finally, all imaging processes —reverse-time migration (RTM), point-spread functions (PSF), and the inversions, have $\mathbf{b}_0$ as input background model.

For the Gauss-Newton Hessian stage of LWIVU, I precompute the Hessian using a PSF layout (Tang and Lee, 2015; Fletcher et al., 2016) obtained by applying Born forward modeling followed by Born adjoint modeling (RTM) to spikes seeded every 15 gridpoints in model space (Figure 2.) Interpolating values of the PSFs corresponding to specific lags (distances with respect to the central point) we can construct columns of the Hessian (for instance, picking the central values of the PSF and interpolating we estimate the diagonal of the Hessian). Its application during the inversion becomes a fast, matrix-like, multiplication (Cabrales-Vargas et al., 2017). I employed the diagonal and six-lag off-diagonal terms (for a total of 13×13) to approximate the Hessian.

The current LWIVU implementation works with the out-of-core solver recently developed in the Stanford Exploration Project by Biondi and Barnier (2017). Adjoint Born modeling and WEMVA incorporate random boundary conditions (RBC) to reduce memory requirements at the expense of extra wavefield propagations (Clapp, 2009; Shen and Clapp, 2011). RBC are incorporated into WEMVA as explained in Cabrales-Vargas (2017). The WEMVA stage of LWIVU is implemented in non-extended domain by maximizing the energy of the migration image.

NUMERICAL RESULTS

All the inversions shown in this report were run for 10 iterations.

Figures 3a and 3b show zooms around the reflector of conventional RTM images of the two-layer model using as input data $\mathbf{\Delta d}$ and $\mathbf{\Delta d}_0$, respectively. Note the small disturbances on the amplitude of the reflector in Figure 3a, between $x = 9000$ m and $x = 13000$ m, despite the fact that the reflector appears to be completely flat in both cases. Figure 4 shows the amplitude extractions at the peak of the reflector revealing that the anomalies have a significant impact.

Figure 5 shows LWI images obtained using as input the migration images of Figure 3. Their corresponding amplitude extractions are compared with the reflectivity, $\mathbf{\Delta r}$, in Figure 6. Similar to the RTM case, we observe amplitude distorsions caused by the anomalies. There are amplitude-based seismic attributes (e.g. Chopra and Marfurt, 2007) that can be sensitive to such amplitude distorsions. They can potentially mask real geologic features or even portray false ones. The consequence in either case is a foul interpretation.

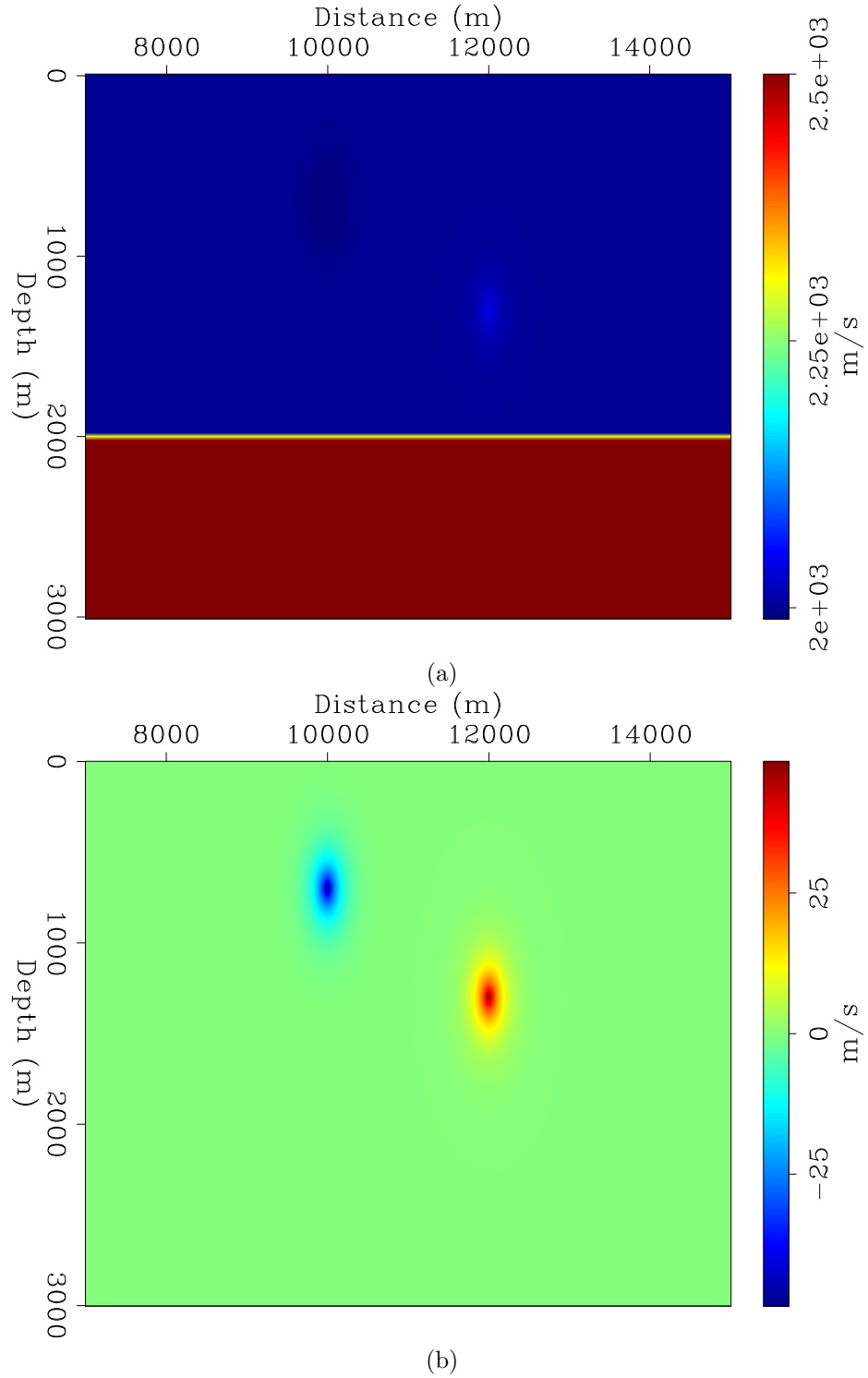

Figure 1:]
(a) Two-layer velocity model with (b) Gaussian anomalies. The peak amplitudes of the anomalies are, from left to right, -50 and 50 m/s approximately. This model constitutes the true subsurface model from where the perturbation of the data is computed. The Gaussian anomalies are centered at $(x = 10000m, z = 750m)$ and $(x = 12000m, z = 1250m)$, and are barely visible in the upper layer. [**ER**]

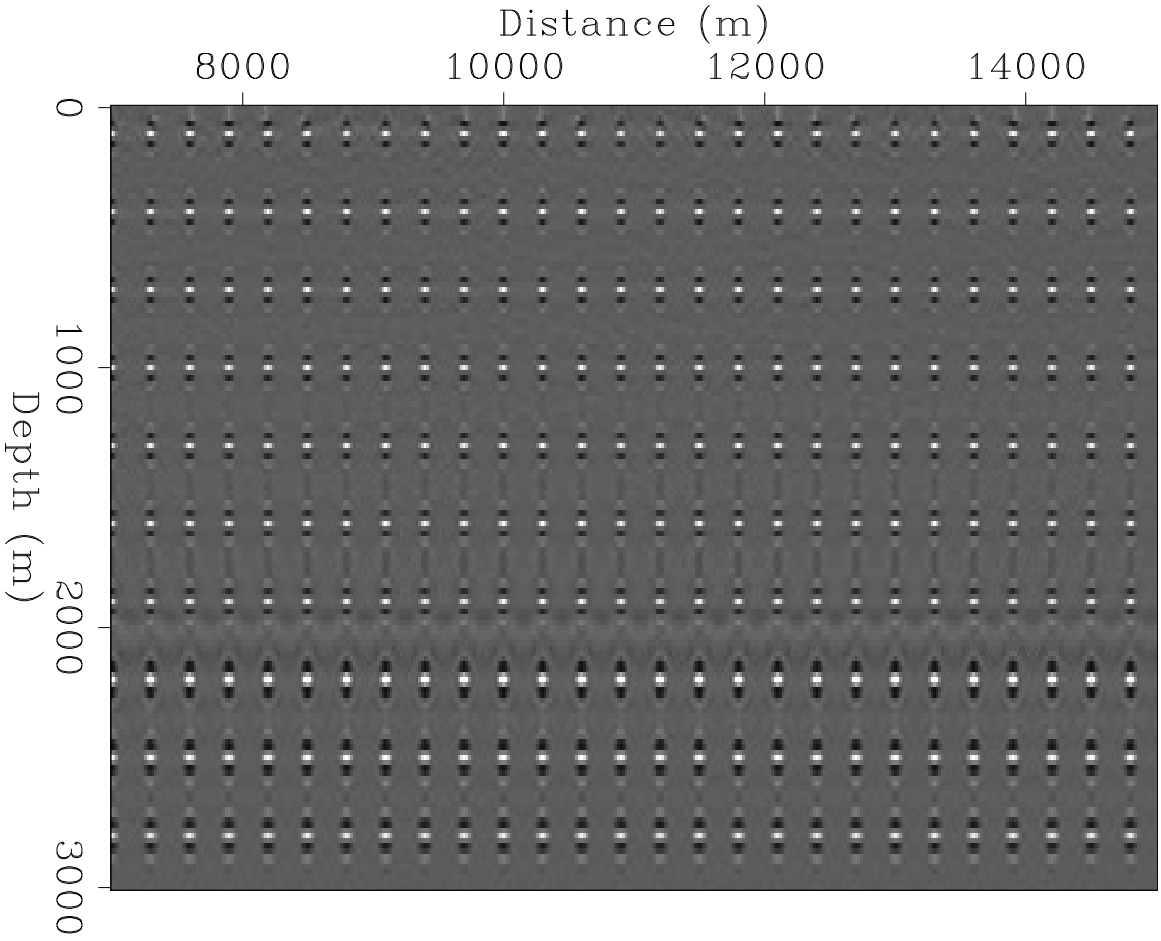

Figure 2: .
]Point-spread functions for the estimation of the Gauss-Newton Hessian [**CR**].

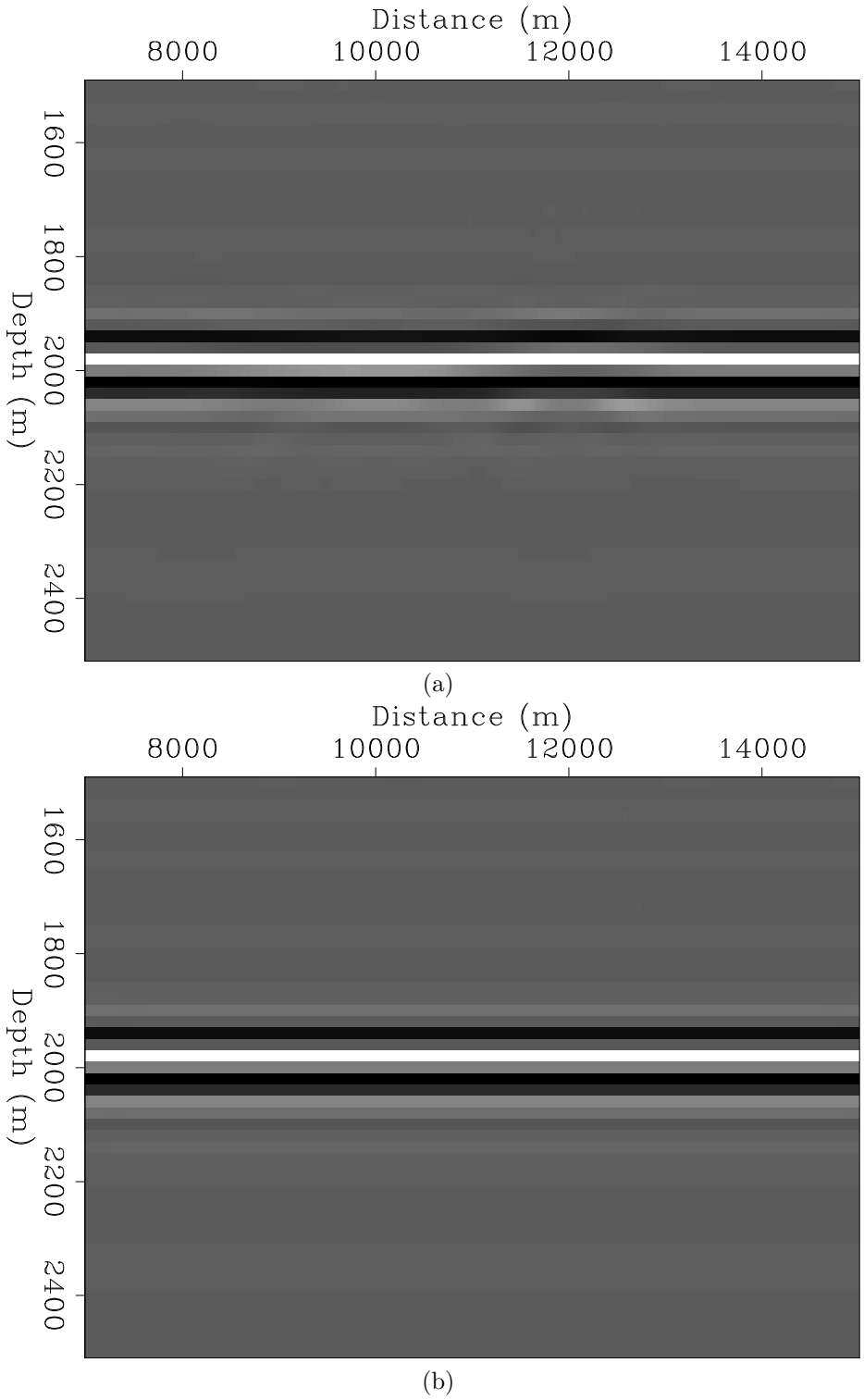

Figure 3:]
(a) RTM image using $\mathbf{\Delta d}$. (b) RTM image using $\mathbf{\Delta d}_0$. Both images were computed using $\mathbf{b}_0$ as background model, and are plotted at the same scale.[**CR**]

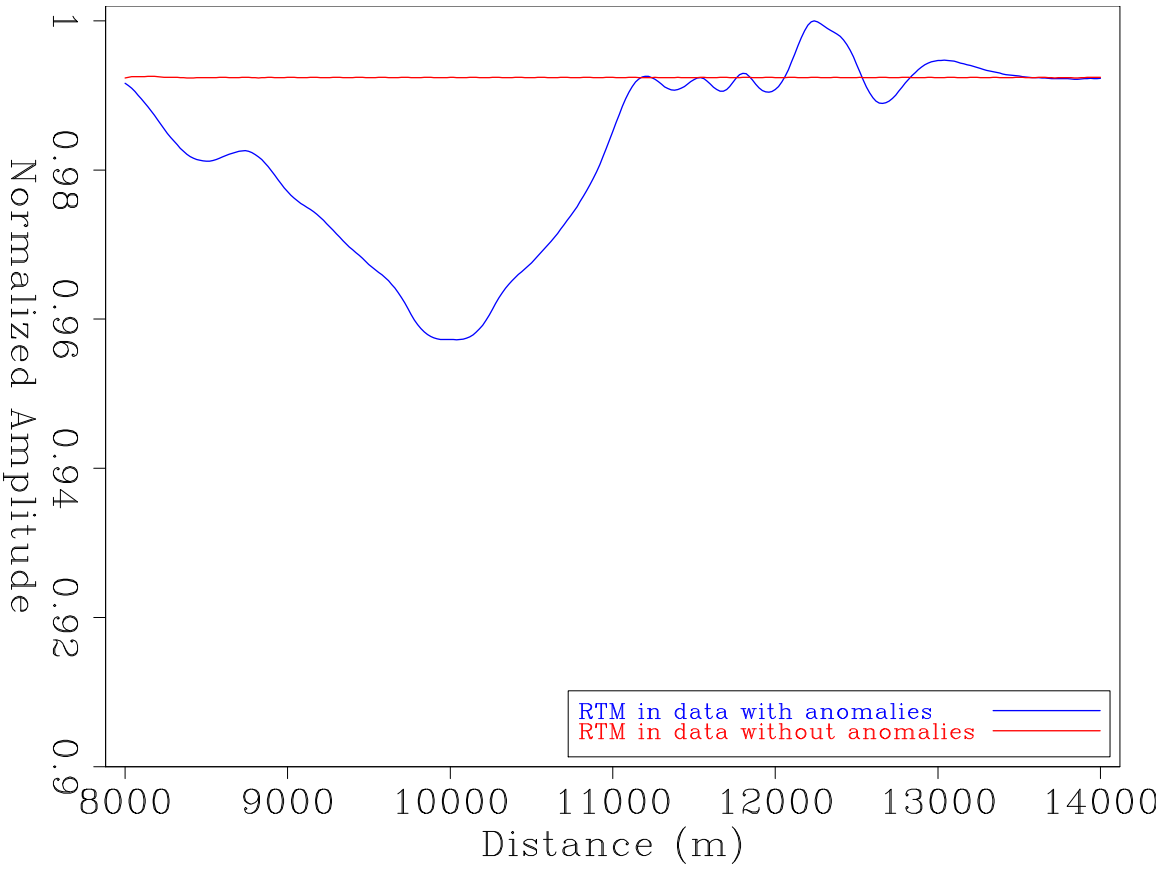

Figure 4:]
Amplitude extractions at the peak of the reflector from RTM images in Figure 3. Amplitudes are normalized. [**CR**]

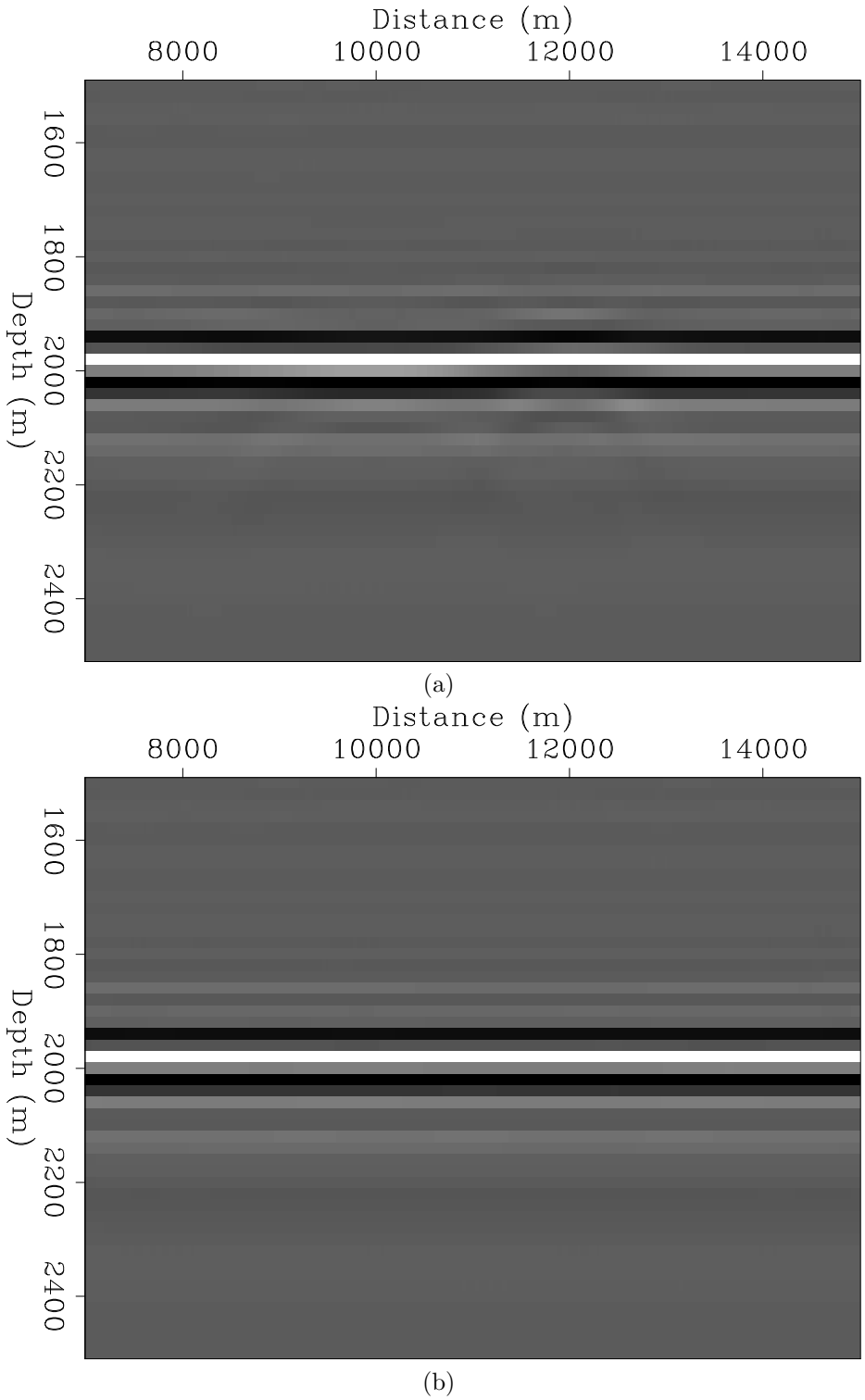

Figure 5:]
LWI images computed using as input RTM images in (a) Figure 3a, and (b) Figure 3b. The images are plotted at the same scale. [**CR**]

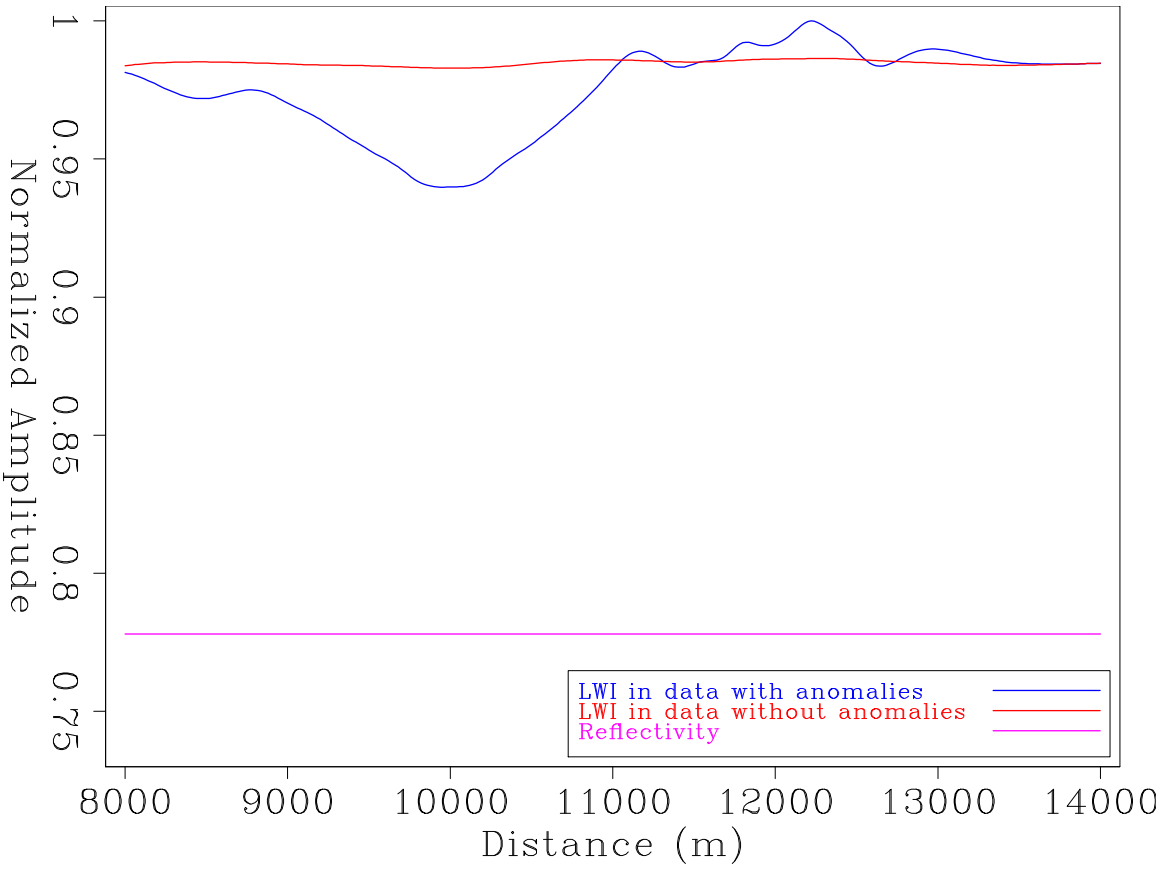

Figure 6:]
Amplitude extractions at the peak of the reflector from LWI images in Figure 5, compared with the true reflectivity. Amplitudes are normalized. [**CR**]

Figure 7 shows the result of the reflectivity component of LWIVU in comparison with conventional LWI. Both images have as input the RTM image computed with $\mathbf{\Delta d}$. The LWIVU computation also requires $\mathbf{\Delta d}$ as input for the WEMVA operator. The parameter λ was set to 2.5. Note that the disturbances in the amplitude are only apparent in the the LWI image. The corresponding amplitude extractions are compared with the true reflectivity in Figure 6, and include the amplitude extraction on the LWI image obtained from the RTM image of Figure 3b, in turn computed with $\mathbf{\Delta d}_0$. Note that the LWIVU amplitude is almost completely corrected for the effects of the anomaly. Moreover, it gets closer to the true reflectivity, possibly because the inaccuracies in the model introduced by smoothing were partially corrected during the WEMVA stage (yet, it is improbable that any of the inversions can exactly match the reflectivity, for the data were synthesized using non-linear modeling instead of Born modeling). Finally, Figure 9 shows the LWIVU perturbation of the background compared with the true anomalies in slowness squared, where we confirm that the LWIVU $\mathbf{\Delta b}$ approximately matches the anomalies.

CONCLUSION AND FUTURE WORK

The numerical experiments shown in this report demonstrate that LWIVU can correct amplitude distorsions introduced by small anomalies in the background model, where we understand by "small" a maximum of $\pm 5\%$ deviation from the true values in order to avoid cycle skipping of the WEMVA operator. Although such distorsions are not likely to affect the interpretation at oil & gas play- and prospect-scale exploration, the detailed assessment of the amplitudes during reservoir characterization can be misled.

More complex models have to be tested with LWIVU. I currently experiment with the Sigsbee A model. At the same time I prepare the necessary components (Born modeling, RTM, WEMVA, etc.) for the 3-D version of the method.

Equation 8 has an unusual structure: The *difference* of two objective functions. One consequence is that, as aforementioned, it is not possible to obtain the forward and the adjoint of the Hessian/WEMVA composed operator because of the minus sign preceeding λ^2. Such minus sign can cause that the objective function becomes non-quadratic, at least in the general case.

If the situation just described proves to be an issue, one alternative is switching from maximization of stacking (or energy) power to differential semblance optimization (DSO) (Symes and Carazzone, 1991). The corresponding LWIVU objective function is

$$\Phi(\mathbf{\Delta r}, \mathbf{\Delta b}; \mathbf{b}_0) = \frac{1}{2}\big\|\mathbf{H\Delta r} - \mathbf{W\Delta b} - \mathbf{\Delta r}_m\big\|_2^2 + \frac{\lambda^2}{2}\big\|\mathbf{D}\big[\mathbf{W\Delta b} + \mathbf{\Delta r}_m\big]\big\|_2^2. \qquad (12)$$

where $\mathbf{D}$ constitutes the DSO operator. Note that the minus sign is no longer because minimization of the DSO term, not maximization, is sought. We can obtain the

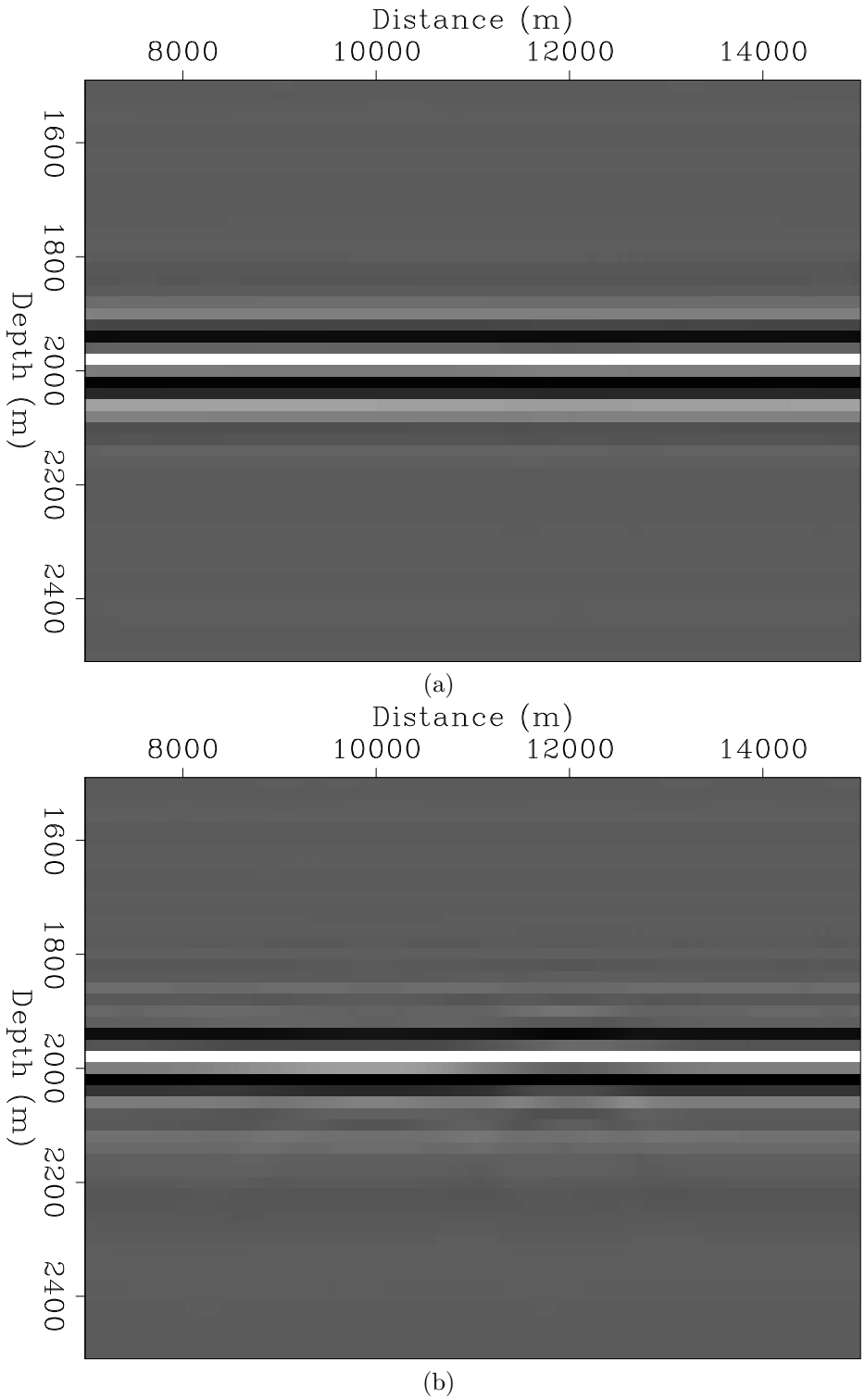

Figure 7:]
(a) LWIVU reflectivity image compared with (b) LWI image. The images are plotted at the same scale. [**CR**]

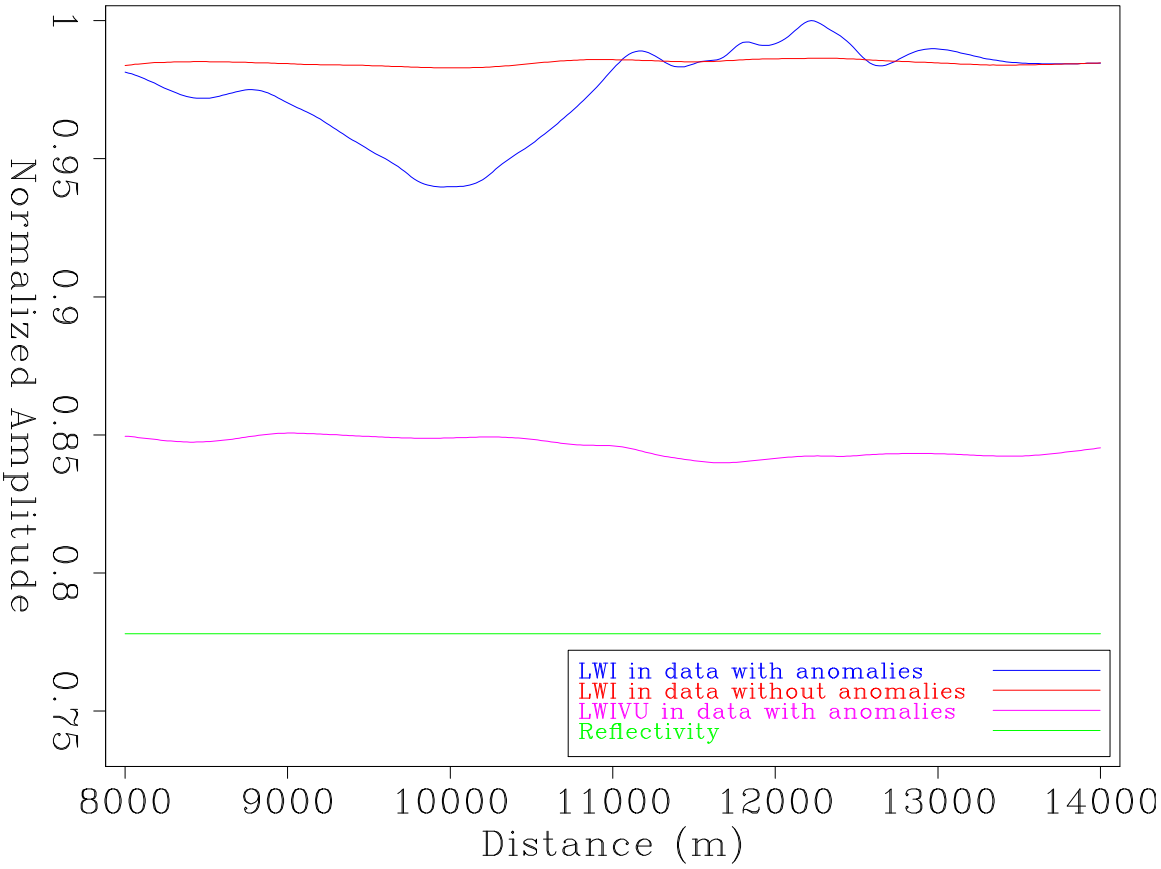

Figure 8:]
Amplitude extractions at the peak of the reflector from the LWIVU reflectivity image (Figure 7a) and the LWI image (Figure 7b), compared with the true reflectivity. Amplitudes are normalized. [**CR**]

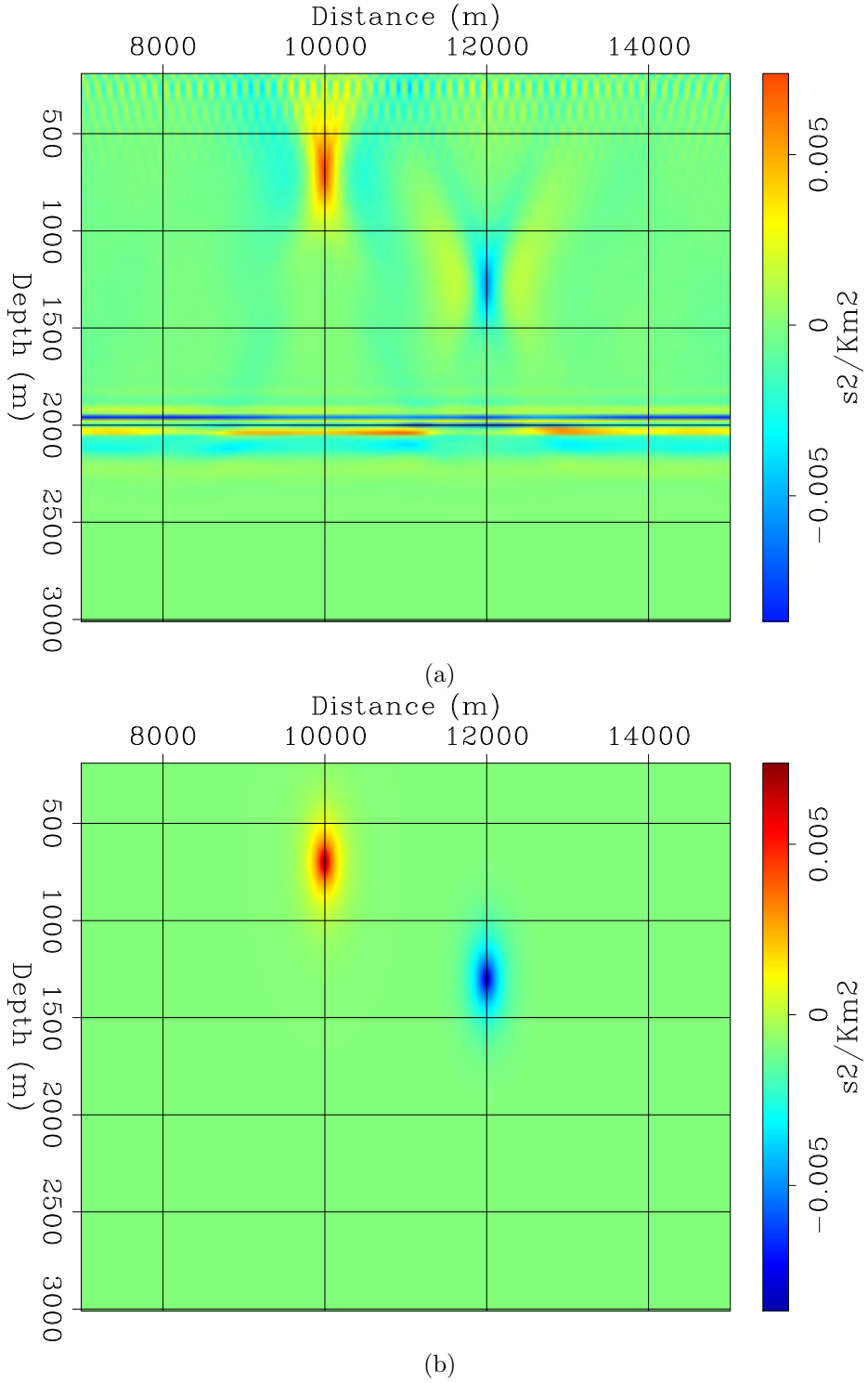

Figure 9:]
(a) Perturbation in the background obtained during LWIVU compared with (b) the true slowness squared anomalies. Gridding lines facilitate comparison. The images are plotted at the same scale. [**CR**]

corresponding normal equations:

$$\begin{bmatrix} \mathbf{H}' & \mathbf{0} \\ -\mathbf{W}' & \lambda \mathbf{W}'\mathbf{D}' \end{bmatrix} \left\{ \begin{bmatrix} \mathbf{H} & -\mathbf{W} \\ \mathbf{0} & \lambda \mathbf{D}\mathbf{W} \end{bmatrix} \begin{bmatrix} \mathbf{\Delta r} \\ \mathbf{\Delta b} \end{bmatrix} - \begin{bmatrix} \mathbf{\Delta r}_m \\ -\lambda \mathbf{D}\mathbf{\Delta r}_m \end{bmatrix} \right\} = \begin{bmatrix} \mathbf{0} \\ \mathbf{0} \end{bmatrix}.$$

Note that this time the matrix-like operators are truly adjoint of each other, unlike equation 10. The caveat of this approach is that equation 12 ought to be implemented in extended domain (subsurface offset), whereas equation 8 operates in non-extended domain.

ACKNOWLEDGMENT

I would like to thank the SEP sponsors for their support, and Petróleos Mexicanos for the financial aid. Special thanks to Ettore Biondi and Guillaume Barnier for their very useful out-of-core linear solver.

REFERENCES

Barnier, G. and A. Almomin, 2014, Tutorial on two-way wave equation operators for acoustic, isotropic, constant-density media: SEP-Report, **155**, 23–56.

Biondi, B., E. Biondi, M. Maharramov, and Y. Ma, 2015, Dissection of the full-waveform inversion hessian: SEP-Report, **160**, 19–38.

Biondi, E. and G. Barnier, 2017, A flexible out-of-core solver for linear/non-linear problems: SEP-Report, **168**, 295–308.

Cabrales-Vargas, A., 2017, Implementing Wave-Equation Migration Velocity Analysis Within Linearized Waveform Inversion with Velocity Updating: Considerations and Challenges : SEP-Report, **170**, 149–156.

Cabrales-Vargas, A., B. Biondi, and R. Clapp, 2016, Linearized Waveform Inversion with Velocity Updating: Theory and first results: SEP-Report, **165**, 63–92.

———, 2017, Our progress towards linearized waveform inversion with velocity updating (LWIVU): SEP-Report, **168**, 151–162.

Chopra, S. and K. Marfurt, 2007, Seismic attributes for prospect identification and reservoir characterization: Society of Exploration Geophysicists & European Association of Geoscientists and Engineers.

Clapp, R., 2009, Reverse time migration with random boundaries: SEG Technical Program Expanded Abstracts, 2809–2813.

Fletcher, R., D. Nichols, R. Bloor, and R. Coates, 2016, Least-squares migation - data domain versus image domain using point spread functions: The Leading Edge, **35**, no. 2, 157–162.

Nemeth, T. and G. Schuster, 1999, Least-squares migration of incomplete reflection data: Geophysics, **64**, no. 1, 208–221.

Schuster, G., 2017, Seismic inversion: Society of Exploration Geophysicists.

Shen, X. and R. Clapp, 2011, Random boundary condition for low-frequency wave propagation: SEG Technical Program Expanded Abstracts, 2962–2965.

Symes, W. and J. Carazzone, 1991, Velocity inversion by differential semblance optimization: Geophysics, **56**, 654–663.

Tang, Y., 2011, Imaging and velocity analysis by target-oriented wavefield inversion: PhD thesis, Stanford University.

Tang, Y. and S. Lee, 2015, Multi-parameter full wavefield inversion using non-stationary point-spread functions: SEG Technical Program Expanded Abstracts 2015, 1111–1115.

Valenciano, A., B. Biondi, and A. Guitton, 2006, Target-oriented wave-equation inversion: Geophysics, **71**, no. 4, A35–A38.